



# Sedation-free pediatric [ $^{18}\text{F}$ ]FDG imaging on totalbody PET/CT with the assistance of artificial intelligence

Xiang Zhou<sup>1</sup> · Song Xue<sup>2,3</sup> · Lianghua Li<sup>1</sup> · Robert Seifert<sup>2</sup> · Shunjie Dong<sup>4</sup> · Ruohua Chen<sup>1</sup> · Gang Huang<sup>1</sup> · Axel Rominger<sup>2</sup> · Jianjun Liu<sup>1</sup> · Kuangyu Shi<sup>2</sup>

Received: 27 March 2024 / Accepted: 21 June 2024

© The Author(s), under exclusive licence to Springer-Verlag GmbH Germany, part of Springer Nature 2024

## Abstract

**Purpose** While sedation is routinely used in pediatric PET examinations to preserve diagnostic quality, it may result in side effects and may affect the radiotracer's biodistribution. This study aims to investigate the feasibility of sedation-free pediatric PET imaging using ultra-fast total-body (TB) PET scanners and deep learning (DL)-based attenuation and scatter correction (ASC).

**Methods** This retrospective study included TB PET (uExplorer) imaging of 35 sedated pediatric patients under four years old to determine the minimum effective scanning time. A DL-based ASC method was applied to enhance PET quantification. Both quantitative and qualitative assessments were conducted to evaluate the image quality of ultra-fast DL-ASC PET. Five non-sedated pediatric patients were subsequently used to validate the proposed approach.

**Results** Comparisons between standard 300-second and ultra-fast 15-second imaging, CT-ASC and DL-ASC ultra-fast 15-second images, as well as DL-ASC ultra-fast 15-second images in non-sedated and sedated patients, showed no significant differences in qualitative scoring, lesion detectability, and quantitative Standard Uptake Value (SUV) ( $P = \text{ns}$ ).

**Conclusions** This study demonstrates that pediatric PET imaging can be effectively performed without sedation by combining ultra-fast imaging techniques with a DL-based ASC. This advancement in sedation-free ultra-fast PET imaging holds potential for broader clinical adoption.

**Keywords**  $^{18}\text{F}$ -FDG · Total-body PET · Ultrafast · Pediatrics · Diagnostic performance

---

Xiang Zhou, Song Xue and Lianghua Li contributed equally to this work.

✉ Jianjun Liu  
jianjun\_liu2018@163.com

<sup>1</sup> Department of Nuclear Medicine, Institute of Clinical Nuclear Medicine, Renji Hospital, School of Medicine, Shanghai Jiao Tong University, Shanghai 200127, China

<sup>2</sup> Department of Nuclear Medicine, Inselspital, Bern University Hospital, University of Bern, Street Freiburgr. 18, Bern 3010, Switzerland

<sup>3</sup> Department of Biomedical Imaging and Image-Guided Therapy, Division of Nuclear Medicine, Medical University of Vienna, Vienna, Austria

<sup>4</sup> College of Health Science and Technology, Shanghai Jiao Tong University School of Medicine, Shanghai, China

## Introduction

[ $^{18}\text{F}$ ]FDG PET imaging has been widely used in clinical and research applications over the past few decades. The application of PET in pediatric diseases has also gradually attracted attention and has become an essential diagnostic tool in the imaging evaluation of pediatric tumors and non-tumor diseases [1]. [ $^{18}\text{F}$ ]FDG PET is used in the diagnosis of pediatric solid tumors, hematological tumors, post-transplant lymphoproliferative disease (PTLD), and fever of unknown origin (FUO) [2–4], and is routinely used for staging, assessing response to treatment, monitoring the course of the disease, and detecting recurrence in many malignancies [5].

Pediatric PET imaging is often performed when patients are sedated to achieve good-quality PET imaging [6]. Because keeping the child still during the examination is not easy, and the motion during scanning would corrupt reconstructions, leaving artifacts in the final image. However,

sedation has the following disadvantages: (1) It will have a potential impact on the neurodevelopment of children [7]; (2) Some children will not cooperate to take sedatives, or after taking sedatives, some children have involuntary movements during the examination. (3) It is also essential to consider the potential effects of sedatives on FDG tracer bio-distribution [8–10] or peripheral-type benzodiazepine receptor imaging [11, 12], especially in early or dynamic PET imaging.

Therefore, some physicians performed clinical studies on PET imaging in children without sedation using long axial field-of-view (FOV) PET/CT [13–15]. However, in the non-sedation state, children will be prone to move during the PET scan period and produce motion artifacts in acquired PET images. Many studies focus on sedation-free pediatric PET imaging, developing techniques for correcting motion-corrupted PET images. Some tracked the motion with external devices [16], but the complex setup might hamper the adoption into clinical routine. Other studies have attempted to extract motion signals directly from raw PET data [17], which may not accurately convey the actual motion amplitude. The limitation of current data-driven methods for PET relates to the CT image used for attenuation and scatter correction (ASC), particularly evident in cases of respiratory motion, which can lead to scatter or attenuation artifacts affecting PET quantification.

Ultra-fast total-body (TB) PET imaging may balance acquisition time and image reconstruction quality from the raw data for signal extraction back to image-based methods [18]. The advent of TB PET made it possible for ultra-fast PET scan [19]. Shi et al. reported that no significant difference were observed in the diagnostic accuracy of adult tumors between scanning 300 s and 30 s ( $P=ns$ ) [20]. Additionally, the motion also presents a problem during the ASC of PET images, especially in the case of ultra-fast PET scans. Emission-based AC is the one possible solution for that. Xue et al. [21] employed a simple way to integrate domain knowledge in deep learning (DL) for computed tomography (CT)-free PET imaging.

Our study explored the value of ultra-fast TB PET and DL-based ASC for sedation-free pediatric PET imaging. We established the feasibility of PET imaging through TB PET rapid scan and PET ASC without sedation.

## Methods

### Patient cohorts

This study analyzed the data of 40 patients with suspected tumors that were referred to the Department of Nuclear Medicine to undergo [ $^{18}\text{F}$ ]FDG PET/CT for tumor diagnosis and

staging from January 2022 to January 2023. The inclusion criteria were as follows: (1) under 4 years old (2) undergo TB PET scan (3) definite surgical pathology or follow-up data. Among them, 35 children were orally sedated 20 min before the PET scan. 5 children did not take any sedatives during the PET scan. The study was approved by the institutional review board of Renji hospital, and the informed consent was obtained from all patients' legal guardians.

### General imaging protocols

All patients fasted for at least 6 h before [ $^{18}\text{F}$ ]FDG administration. The list-mode PET data were acquired using a TB PET/CT scanner with 194-cm-long axial FOV (uEXPLORER, United Imaging Healthcare, Shanghai, China) 60 min after [ $^{18}\text{F}$ ]FDG injection 3.7MBq/kg [0.1 mCi/kg] activity per body weight). The acquisition time was 300 s. All PET imaging was reconstructed with the same parameters: time of flight [22] and point spread function modeling; ordered subset expectation maximization algorithm with 2 iterations and 20 subsets; matrix,  $192 \times 192$ ; slice thickness, 2.89 mm; FOV, 600 mm (pixel size,  $3.125 \times 3.125 \times 2.89$  mm) with a Gaussian post-filter (3 mm). Low-dose CT scans of the whole body were obtained by uEXPLORER (tube current 10 mA, voltage 100 kV, rotation time 0.5s, pitch 1.0125, collimation  $80 \times 0.5$  mm) were reconstructed in a  $512 \times 512$  matrix for ASC.

### Imaging protocols for patients under sedation

We define “fast-scan-time” (FST) as a time window featuring randomly sampled full-count data, simulating the fast imaging conditions relevant to practical scenarios. PET images of 35 sedated children (administered chloral hydrate orally at 30–50 mg/kg) were reconstructed from FST data captured at various intervals (300s, 60s, 30s, 15s, 10s, 5s). Prior to PET data acquisition, a CT scan was conducted for ASC. For each FST interval, both CT-ASC PET images and non-corrected (NASC) PET images were obtained; for instance, FST-300s CT-ASC represents PET imaging reconstructed from 300 FST data with CT-based ASC applied.

### Imaging protocols for sedation-free patients

Five children were initially subjected to PET/CT scans while non-sedated, followed by subsequent CT-free PET scans under sedation. The standard protocol for PET scans is set at 300 s in a non-sedated context. However, the scanning process is subject to interruption should the patient display excessive movement or an inability to maintain cooperation. The minimum scan duration achieved among these non-sedated children was 60 s. PET imaging frames

were reconstructed based on 5-second intervals of counts. The PMOD software was utilized to identify a period of three consecutive frames (15 s) where the child remained motionless, then the reconstruction was performed with the counts from the identified motionless time window. Reconstructed NASC PET imaging was collected at FST-15s and FST-300s.

### Deep learning-based correction

We leveraged the framework introduced in our previous work on DL-based AC within the realm of ultra-fast PET imaging [21]. This method offers a straightforward means of

incorporating domain knowledge into DL for CT-free PET imaging. Particularly, as depicted in Fig. 1, we customized the generative adversarial network to estimate the anatomy-dependent correction map, calculated from the FST-300s CT-ASC PET image, with the input being the non-corrected ultra-fast FST-15s NASC PET image. The selection of FST-15s for this process was based on our thorough evaluation of ultra-fast PET imaging. Our training phase involved a dataset of 30 sedated patients, chosen randomly from a total cohort of 35. We then validated our model on the remaining 5 patients from the sedated group, and further tested on the 5 non-sedated patients.

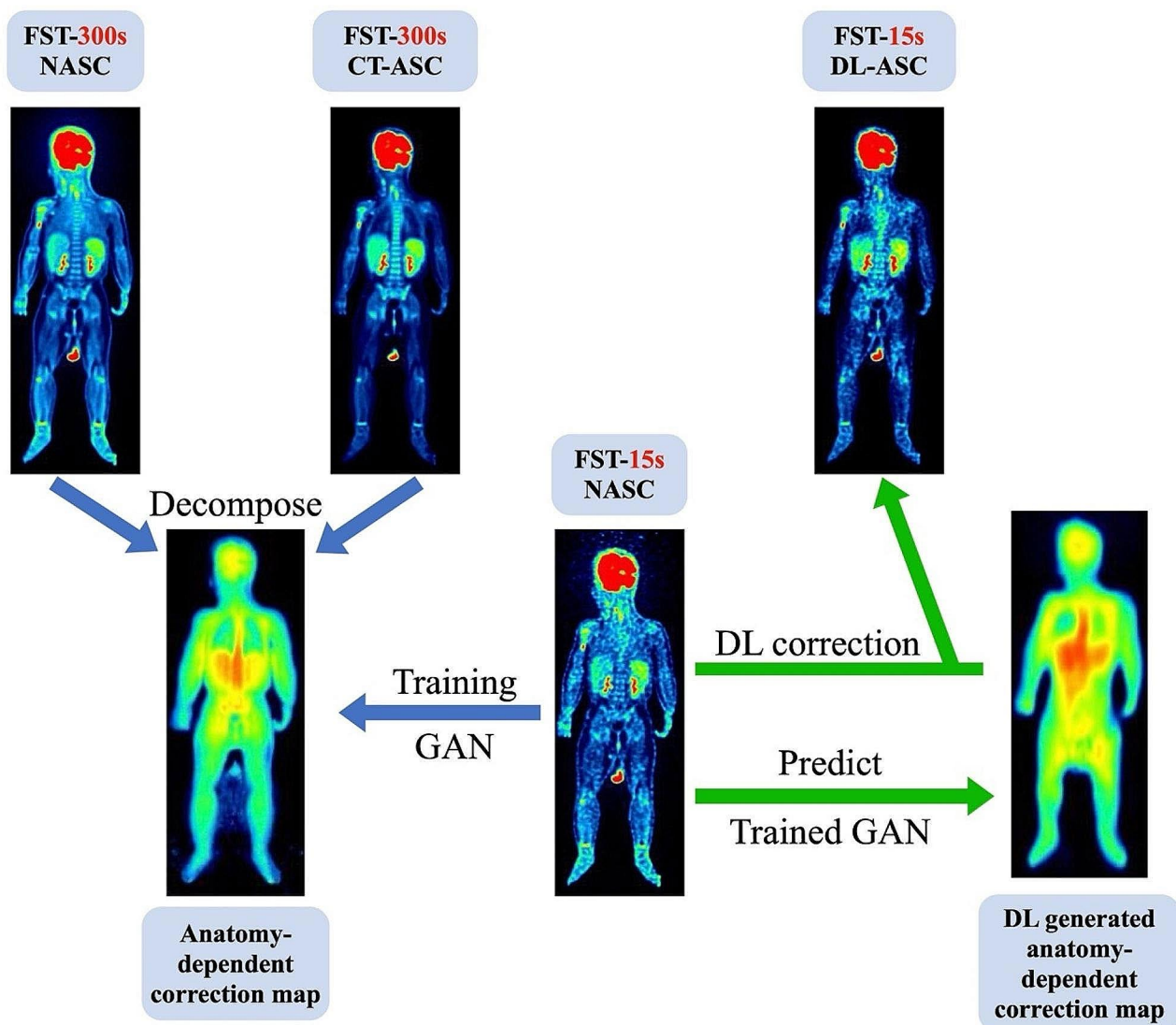


**Fig. 1** General protocol of our customized deep learning method for attenuation and scatter correction. We employed a modified generative adversarial network to derive an anatomy-specific correction map from a standard full-time PET image (300s), denoted as FST-300s

CT-based attenuation and scatter corrected (CT-ASC) PET, alongside FST-300s NASC PET. The input to the network was the non-corrected ultra-fast PET image (15s), specifically FST-15s NASC

**Table 1** Demographic information of patients' data

characteristics	No. of patients(%) (n=40)
Age (years)	
Mean $\pm$ SD	2.3 $\pm$ 1.0
Median (range)	2.4(0.5–3.9)
Gender	
Male	13
Female	27
BMI	
Mean $\pm$ SD	17.1 $\pm$ 2.3
Median (range)	17.5(14.3–21.3)
Injected dose per weight (MBq/Kg)	
Mean $\pm$ SD	3.7 $\pm$ 0.1
Median (range)	3.7(3.5–4.1)
Delay between injection and acquisition (min)	
Mean $\pm$ SD	60.0 $\pm$ 5.2
Median (range)	59.5(50–71)
Glucose blood level (mmol/L)	
Mean $\pm$ SD	4.6 $\pm$ 0.6
Median (range)	4.7(3.5–5.9)
Pediatrics disease	
Neuroblastoma	16
PTLD	9
sarcoma	8
Lymphoma	4
Leukaemia	3

## Evaluation

### Qualitative evaluation

The quality of PET images was independently assessed by two board-certified nuclear medicine physicians with over a decade of experience (X.Z. and R. C.). Employing a 5-point scale (Supplementary Table S1), they evaluated the overall image quality. Images receiving a score of 2 or more were deemed diagnostically adequate. During the evaluation, the physicians were blinded to patient history and acquisition time, and the order of image presentation was randomized to minimize potential bias.

### Quantitative evaluation

To evaluate the efficacy of ultra-fast PET imaging, two board-certified nuclear medicine physicians (X.Z. and R. C.) utilized PMOD software to manually identify circular regions of interest (ROIs) within the aorta lumen and the normal parenchyma of the right liver lobe, each approximately 2.0 cm in diameter (ranging from 1.5 to 2.5 cm). Lesions were also identified and outlined. This process facilitated the measurement of Standardized Uptake Values (SUV) and the subsequent statistical analysis of imaging

**Table 2** Scores of qualitative assessments of ultra-fast PET image quality

MIP	Reader 1		Reader 2		Lesion	Reader 1		Reader 2	
	Mean + SD	Mean + SD	Mean + SD	Mean + SD		Mean + SD	Mean + SD		
300s	5.0 $\pm$ 0.1	5.0 $\pm$ 0.2	300s	5.0 $\pm$ 0.1	5.0 $\pm$ 0.1				
60s	4.1 $\pm$ 0.4	4.4 $\pm$ 0.5	60s	4.3 $\pm$ 0.5	4.7 $\pm$ 0.6				
30s	2.8 $\pm$ 0.3	3.2 $\pm$ 0.2	20s	3.0 $\pm$ 0.2	3.3 $\pm$ 0.4				
15s	2.2 $\pm$ 0.2	2.5 $\pm$ 0.3	15s	2.5 $\pm$ 0.2	2.7 $\pm$ 0.3				
10s	1.5 $\pm$ 0.2	1.8 $\pm$ 0.3	10s	1.6 $\pm$ 0.3	1.8 $\pm$ 0.4				
5s	1.3 $\pm$ 0.2	1.4 $\pm$ 0.3	5s	1.6 $\pm$ 0.4	1.6 $\pm$ 0.3				

parameters, including SUVmax, SUVmean, and the tumor-to-background ratio (TBR). TBR was derived by dividing the lesion SUVmax by the liver SUVmean. Lesions with SUVmax > 2.5 or TBR > 1 were identified as suspected lesions. Furthermore, global physical metrics were calculated in comparison to FST-300s CT-ASC PET imaging. These metrics included structural similarity index measurement (SSIM), signal-to-noise ratio (SNR), and voxel-wise root mean squared error (RMSE).

### Statistical analysis

Statistical analyses were conducted using SPSS 16.0 Statistics. The inter-reader agreement was evaluated through linearly weighted kappa coefficient analysis. A paired samples t-test was applied for objective measurement comparisons, while a chi-squared test was utilized to compare lesion detection rates across groups.  $P < 0.05$  was considered statistically significant.

## Results

### Patient cohorts

Table 1 summarizes characteristics of the pediatric patient cohort, comprising 40 individuals (13 males, 27 females) with a mean age of 28 months (range: 0.5 to 3.9 years). The cohort included 16 patients with neuroblastoma, 9 with PTLD, 8 patients with sarcoma, 4 with lymphomas and 3 patients with leukaemia.

### Qualitative evaluation of ultra-fast PET image quality

All imaging used to evaluate ultra-fast image quality was CT-ASC PET imaging. For reference, the FST-300s group achieved an average score of 5. Groups with FST exceeding 15 s (FST-60s, FST-30s, and FST-15s) satisfied clinical standards, scoring over 2, whereas the other groups (FST-10s and FST-5s) exhibited substandard quality (Table 2).

Exemplary MIP and tomographic images, showcasing liver lesions and lymph node metastases, are presented in Figs. 2 and 3, respectively.

Additionally, image quality was also qualitatively assessed based on lesion detectability. In the FST-300s group, 74 suspicious lesions (diagnosis based on  $^{18}\text{F}$ -FDG PET/CT imaging) were identified in 30 sedated patients, while the FST-15s group identified 72, with discrepancies in 2 lesions. These two lesions were either smaller than 1 cm or had an SUV<sub>max</sub> below 2.5, and both originated from the liver (Fig. 4). According to the follow-up and postoperative pathological results, 94 lesions were found in 30 patients, 27 benign, and 67 malignant. Calculation of the diagnostic performance of the 2 groups is based on the lesions. The FST-300s group achieved a sensitivity of 92.5%, specificity of 55.6%, and overall accuracy of 81.9%, compared to the FST-15s group's 89.6% sensitivity, 55.6% specificity, and 79.8% accuracy. No significant statistical differences were noted between these groups ( $P=ns$ ) (Supplementary Table S2).

### Quantitative evaluation of ultra-fast PET image quality

Table 3 presents the quantitative evaluation of ultra-fast PET image quality, focusing on clinical features including SUV<sub>max</sub>, SUV<sub>mean</sub> and TBR. The analysis reveals that groups with FST over 15 s (FST-60s, FST-30s, and FST-15s) matched the reference FST-300s group in SUV<sub>max</sub>, SUV<sub>mean</sub> (for mediastinum, liver and lesions), and TBR (for lesions) with no significant differences ( $P=ns$ ). Conversely, shorter FST groups (FST-10s and FST-5s) showed significantly different results, especially in SUV<sub>max</sub> for

mediastinum and liver ( $P<0.001$ ). Evaluations involving physical metrics (SSIM, SNR and RMSE) are detailed in Supplementary Table S3.

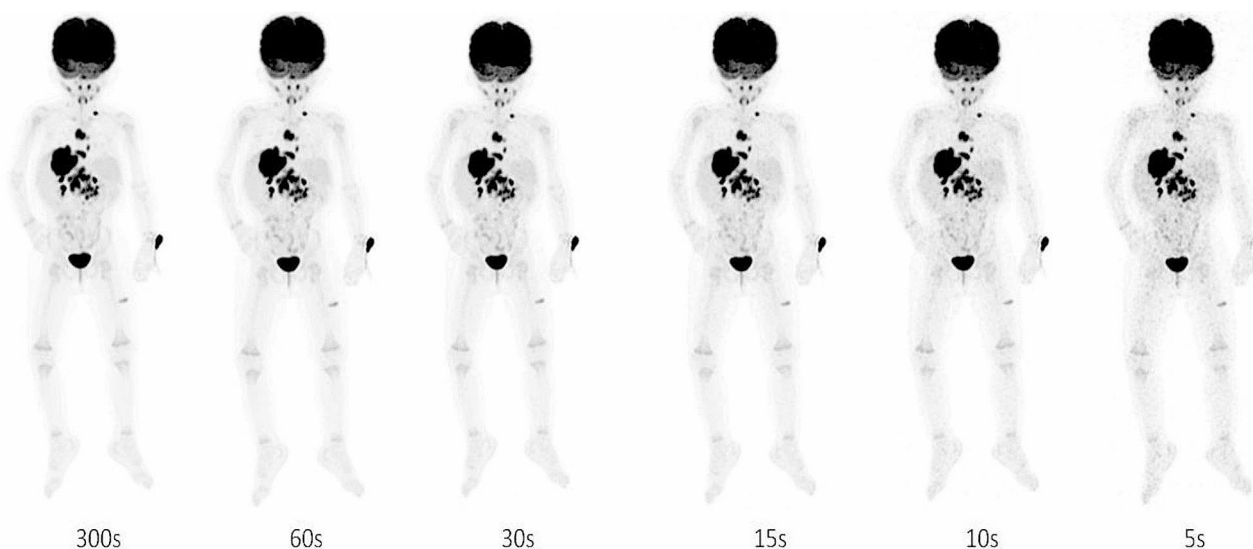
### Evaluation of CT-free PET image quality on sedated patients

Figure 5. A-B demonstrates that the SUV values derived from lesions in five test subjects exhibit no significant disparities between CT-ASC and DL-ASC images (SUV<sub>max</sub>:  $P=0.21$ , SUV<sub>mean</sub>:  $P=0.44$ ). Supplementary Figure S1 details the quantitative accuracy of these images, as assessed using established physical metrics.

In terms of qualitative image quality, DL-ASC images demonstrate significantly superior clarity and detail compared to CT-ASC images for visual assessment ( $P=ns$ ), achieving an average score of 3.5, as documented in Supplementary Table S4. Additionally, Supplementary Figure S1 provides representative results of CT-ASC versus DL-ASC PET imaging in a sedated pediatric patient.

### Evaluation of CT-free PET image quality on non-sedated patients

Figure 5. C-D demonstrates that lesions identified from NASC PET imaging show no significant differences in SUV values, whether the patient is sedated (S/NASC) or not (NS/NASC) ( $P=0.97$  for SUV<sub>max</sub> and  $P=0.08$  for SUV<sub>mean</sub>). Meanwhile, quantification of lesions from sedated CT-ASC and non-sedated DL-ASC images reveals no significant differences. Figure 6 presents the comparison of CT-ASC and DL-ASC PET imaging in a non-sedated pediatric patient. Notably, Lesion 1, located in the abdominal cavity, is more



**Fig. 2** Maximum intensity projection imaging of a 1-year-old child, reconstructed from fast-scan-time at different levels (300s, 60s, 30s, 15s, 10s, 5s)

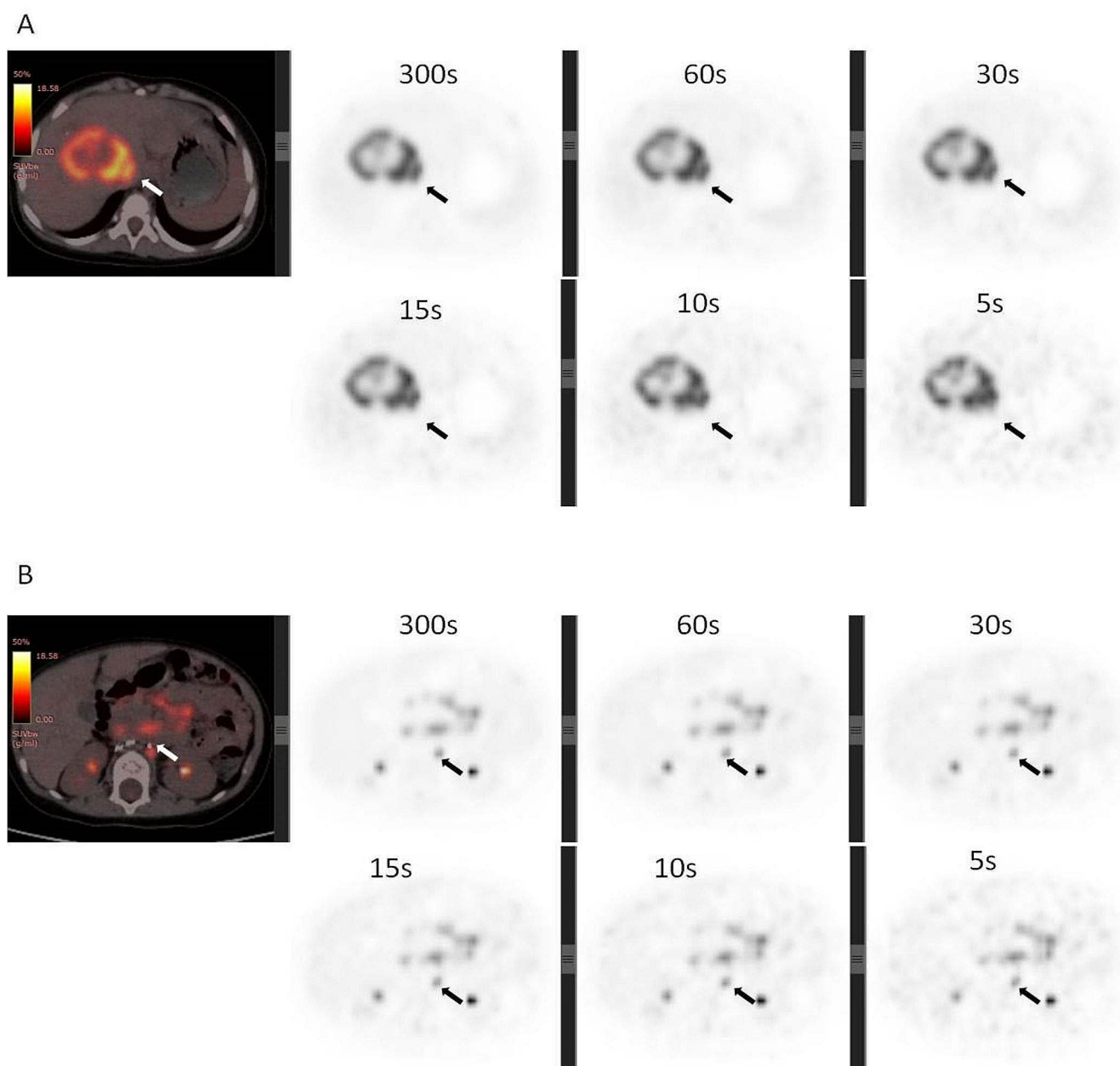


**Fig. 3** Tomographic images of lesions in a 22-month-old child with neuroblastoma, reconstructed from fast-scan-time at different levels (300s, 60s, 30s, 15s, 10s, 5s). **(A)** Arrows indicate liver lesions. The long diameter of liver lesion is 51 mm. SUVmax (SUVmean) of 300, 60, 30, 15, 10, 5, 2s are 13.1(4.7), 13.4(4.7), 13.1(4.6), 13.8(4.7),

13.0(4.7), 13.6(4.7), 17.3(4.7), respectively. **(B)** Arrows indicate the left para-aortic lymph node. The long diameter of the lymph node is 5 mm. SUVmax (SUVmean) of 300, 60, 30, 15, 10, 5, 2s are 2.8(2.6), 2.8(2.5), 3.0(2.5), 3.1(2.6), 3.7(3.0), 3.1(2.8), respectively

discernible in the DL-ASC image due to enhanced contrast, unlike its appearance in the NASC image. Conversely, Lesion 2, located at the thoracic vertebra, is detectable in both NASC and DL-ASC images. However, there is a significant discrepancy in the SUV values between these two methods, with the DL-ASC imaging aligning more closely with the reference values from the FST-300 CT-ASC sedated case. Comprehensive quantitative evaluation of mediastinum, liver and lesions are shown in Table 4. Detailed results

of the qualitative evaluation are available in Supplementary Table S6.

## Discussion

Fast imaging has extensive demand in PET examination of many types of patients [23], such as uncooperative children, cancer patients who cannot tolerate pain, and patients with

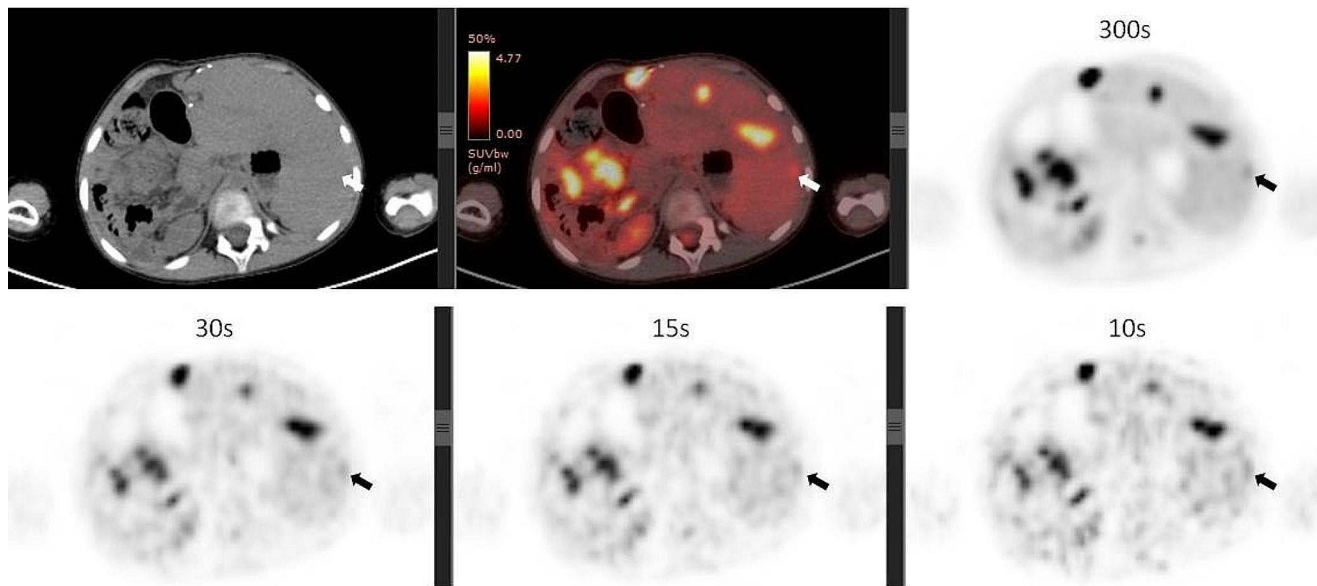


**Fig. 4** A 32-month-old child with posttransplant lymphoproliferative disorders (PTLD) after liver transplantation. The images showed lesions in the liver for the 300s, 30s, 15s, 10s. We can diagnose the

liver lesion that arrow indicate in 300s, but depiction of liver lesion was arguable in 10–30 s

**Table 3** Quantitative evaluation of ultra-fast PET image quality with clinical features

FST	Mediastinum		Liver		Lesions		
	SUVmax	SUVmean	SUVmax	SUVmean	SUVmax	SUVmean	TBR
300s	0.86 ± 0.19	0.69 ± 0.04	1.1 ± 0.3	1.02 ± 0.26	7.07 ± 3.98	3.77 ± 2.03	7.21 ± 4.48
60s	0.85 ± 0.14 ( <i>P</i> =ns)	0.66 ± 0.05 ( <i>P</i> =ns)	1.17 ± 0.22 ( <i>P</i> =ns)	1.03 ± 0.23 ( <i>P</i> =ns)	7.06 ± 3.96 ( <i>P</i> =ns)	3.72 ± 1.98 ( <i>P</i> =ns)	6.92 ± 4.13 ( <i>P</i> =ns)
30s	0.86 ± 0.14 ( <i>P</i> =ns)	0.69 ± 0.08 ( <i>P</i> =ns)	1.17 ± 0.23 ( <i>P</i> =ns)	0.96 ± 0.23 ( <i>P</i> =ns)	7.05 ± 3.91 ( <i>P</i> =ns)	3.71 ± 1.99 ( <i>P</i> =ns)	7.59 ± 4.58 ( <i>P</i> =ns)
15s	0.85 ± 0.14 ( <i>P</i> =ns)	0.7 ± 0.11 ( <i>P</i> =ns)	1.23 ± 0.31 ( <i>P</i> =ns)	0.97 ± 0.24 ( <i>P</i> =ns)	7.15 ± 3.97 ( <i>P</i> =ns)	3.71 ± 1.95 ( <i>P</i> =ns)	7.50 ± 4.47 ( <i>P</i> =ns)
10s	0.96 ± 0.14 ( <i>P</i> <0.001)	0.74 ± 0.05 ( <i>P</i> =ns)	1.29 ± 0.21 ( <i>P</i> <0.001)	0.95 ± 0.17 ( <i>P</i> =ns)	7.20 ± 3.96 ( <i>P</i> =0.043)	3.89 ± 2.09 ( <i>P</i> =0.038)	7.98 ± 4.83 ( <i>P</i> =0.033)
5s	1.33 ± 0.27 ( <i>P</i> <0.001)	0.78 ± 0.11 ( <i>P</i> =0.045)	1.75 ± 0.33 ( <i>P</i> <0.001)	1.14 ± 0.24 ( <i>P</i> =0.041)	7.31 ± 4.12 ( <i>P</i> =0.035)	3.80 ± 1.95 ( <i>P</i> =ns)	7.29 ± 4.44 ( <i>P</i> =ns)

Fast-scan-time (FST): Time window with randomly sampled full-count data, simulating the fast-imaging conditions of practical interest

mental or neurological abnormalities that cannot control their behavior. This is particularly true for pediatric patients, where the common practice of sedation poses certain disadvantages. Our study investigated the minimum feasible scanning time for children, employing DL-based AC to facilitate sedation-free pediatric [<sup>18</sup>F]FDG imaging in total body PET/CT.

Our qualitative and quantitative evaluation of image quality across different FSTs from 5 s to 300 s revealed that a minimum of 15 s is required to meet basic clinical standards. This finding aligns with other studies, such as Zhang Y et al. [20] and Ying-Ying Hu et al. [24], which also support the adequacy of a 15-second scan for basic image quality in pediatric ultra-fast TB PET imaging.

Our examination of the detectability of suspicious lesions indicated that there was no notable difference between the FST-15s and the standard FST-300s modalities. This was consistent except in cases of lesions smaller than 1 cm in diameter or with an SUVmax below 2.5, all of which were in the liver. In clinical settings, the diagnosis of liver lesions is typically corroborated using MRI or ultrasound, ensuring that these lesions are not overlooked. A Total-body PET acquisition time of 3 to 5 min is recommended to facilitate the detection of small liver lesions when suspicious lesions are found on MRI. When no liver lesion is detected in MRI or US, we can shorten the collection time to achieve an ultrafast scan.

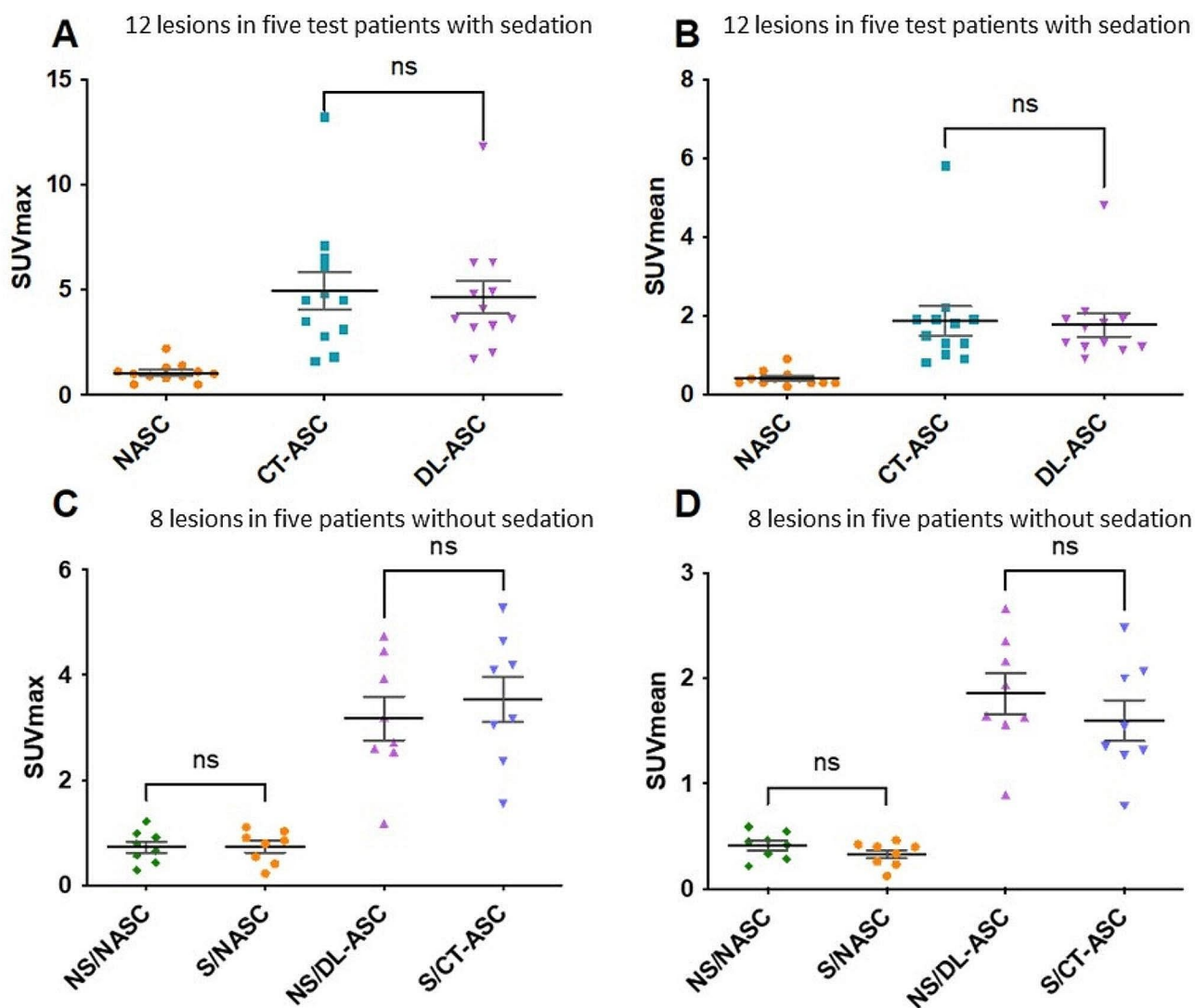


**Fig. 5** Comparisons of lesion SUVmean and SUVmax under no attenuation and scatter correction (NASC), CT attenuation and scatter correction (CT-ASC), and deep learning attenuation and scatter correction (DL-ASC), on sedated and non-sedated test dataset (S/NS). Compari-

son of the lesion SUVmax (A) and SUVmean (B) with 15s FST on sedated patients, and SUVmax (C) and SUVmean (D) on non-sedated patients. DL: deep learning; CT: computerized tomography

Our study also explored the feasibility of 15-second non-sedated PET imaging in children. Challenges include child's unpredictable movement during the scan and the positional discrepancies between CT and PET scans. To address this, we engaged five children in continuous scans ranging from 60 to 300 s without sedation. Analysis via PMOD software confirmed that all children could maintain a static position for at least 15 s. Future research will focus on developing AI software to automatically identify and extract PET data from static positions.

Accurate quantification of PET imaging necessitates ASC, to compensate for photon pair losses due to scattering and photoelectric absorption. However, discrepancies

between CT and PET scans can result in inaccurate corrections, especially for non-sedated patients. To mitigate this issue, our study employed a decomposition-based method [21] designed to extract low-frequency, anatomy-specific information from NASC PET data, which can be applied for correction. Particularly in this ultra-fast imaging scenario, we were able to leverage the richer information from FST-300s scans, to guide the model to estimate the correction map from FST-15s NASC PET image, thereby enhancing the generated image quality (Supplementary Table S7 & Figure S3).

Our research utilized a model trained on a homogeneous and limited amount of dataset using a single scanner and



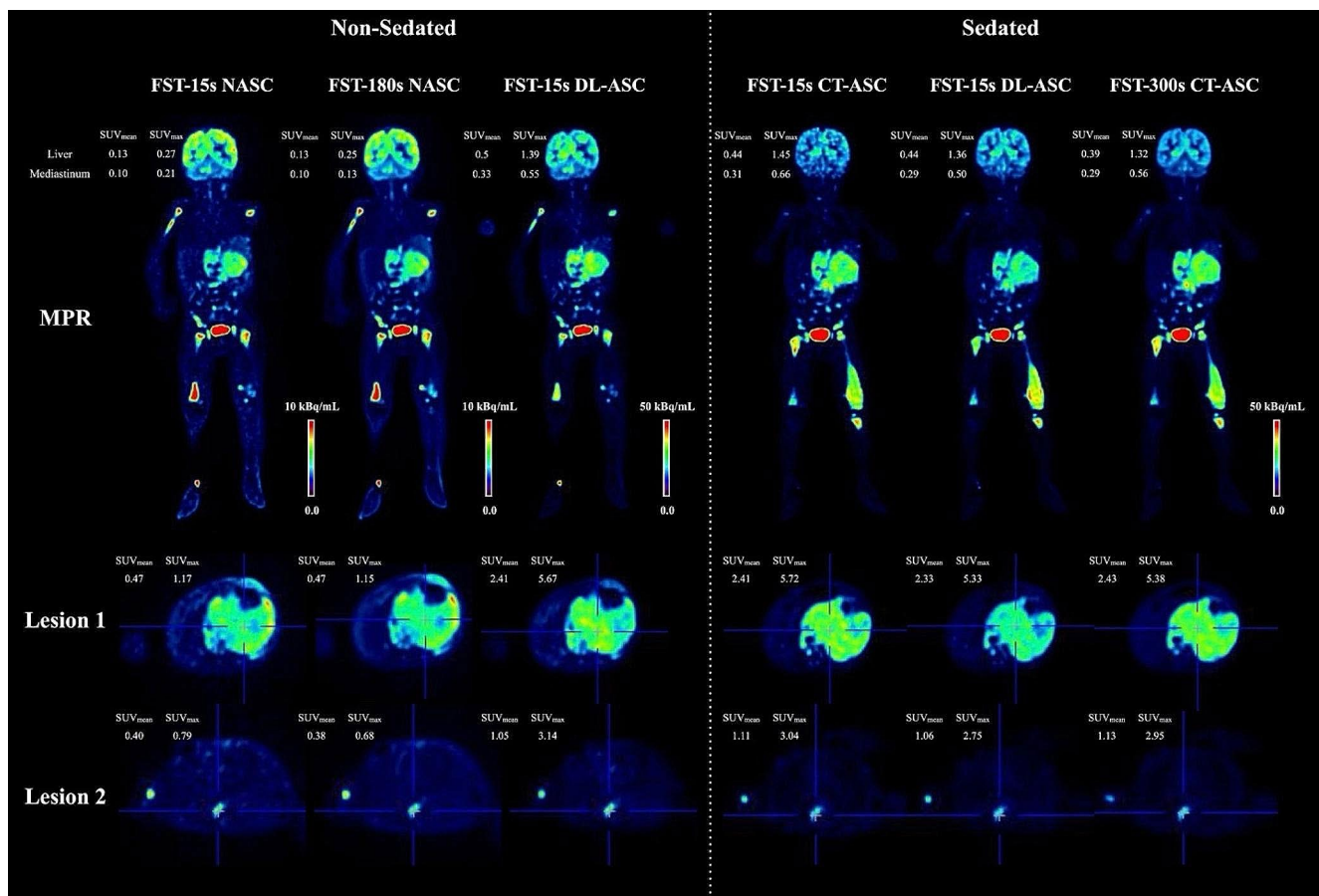


**Fig. 6** 15s ultra-fast DL PET image under non-anesthesia compared to the CTC PET image under anesthesia. A 23-month-old female with multiple metastases of neuroblastoma. In the non-anesthetic PET scan images (three columns on the left), the figure showed the total body MPR images without attenuation correction for 15s, full-time scan (180s) without attenuation correction, and artificial intelligence-assisted attenuation correction. The PET images of typical lesions 1

and lesion 2 were shown in the transversesectional position. Lesion 1 was a large primary tumor in the abdominal cavity, about 20×17 mm in size. Lesion 2 is a bone metastatic tumor, about 12×6 mm in size. as well as SUVmax/SUVmean of mediastinal, liver, and typical lesions were shown in this figure. PET scan images at the anesthesia state were shown in three columns on the right. From left to right, the images were 15s CTC, 15s DL, and full-time (300s) CTC PET

**Table 4** Quantitative evaluation of CT-free PET image quality on non-sedated patients

Correction	Mediastinum		SUVmax	Liver		Lesions	
	SUVmax	SUVmean		SUVmean	SUVmax	SUVmean	TBR
Non-corrected	0.86 ± 0.19	0.69 ± 0.04	1.1 ± 0.3	1.02 ± 0.26	7.07 ± 3.98	3.77 ± 2.03	7.21 ± 4.48
DL-corrected	1.33 ± 0.27	0.78 ± 0.11	1.75 ± 0.33	1.04 ± 0.24	7.31 ± 4.12	3.80 ± 1.95	7.29 ± 4.44

tracer, which may not be ideal for robust DL development. However, our preliminary findings validated the potential of our initial hypothesis. This proof-of-concept underscores the importance of designing more realistic studies in the future, incorporating larger and more diverse datasets that encompass a range of centers, scanners, tracers, diseases, and body regions. Limitations of the study are the amount and variety data included this study. Future research should broaden the scope to include larger dataset, diverse diseases, and other radiotracers like <sup>68</sup>Ga and <sup>11</sup>C for ultra-fast PET imaging in non-sedated children. Furthermore, deep learning-based dose reduction techniques [25] will also be

incorporated to reduce the injected dose for ultra-fast PET imaging, or further reduce the acquisition time.

### Conclusion

This research establishes the feasibility of 15-second ultra-fast TB PET scans for pediatric oncology diagnosis. It demonstrates that pediatric PET imaging can be performed without sedation, utilizing ultra-fast imaging techniques combined with a DL-based AC algorithm. This pioneering effort in sedation-free ultra-fast PET imaging paves the way

for its wider clinical application and fosters further advancements in PET imaging technology.

**Supplementary Information** The online version contains supplementary material available at <https://doi.org/10.1007/s00259-024-06818-3>.

**Funding** This work was supported by in part by the National Key Research and Development Program of China (Grant No. 2020YFA0909000 and 2021YFA0910000), the National Natural Science Foundation of China (Grant No. 81571710).

**Data availability** The data could be obtained from the corresponding author upon request.

## Declarations

**Competing interests** Axel Rominger and Kuangyu Shi are editors of *European Journal of Nuclear Medicine and Molecular Imaging*.

**Ethical approval** All procedures were performed in accordance with the principles of the 1964 Declaration of Helsinki and its later amendments or comparable ethical standards. The study design and exemption from informed consent were approved by the Institutional Review Board of the Ren Ji Hospital.

**Consent to participate** The informed consent was waived.

**Consent for publication** Not applicable.

## References

- Alavi A, Houshmand S, Werner TJ, Zaidi H. Potential applications of PET-Based Novel quantitative techniques in Pediatric diseases and disorders. *PET Clin.* 2020;15:281–4. <https://doi.org/10.1016/j.cpet.2020.03.010>
- Xu YF, Yang JG. Roles of F-18-fluoro-2-deoxy-glucose PET/Computed tomography scans in the management of post-transplant lymphoproliferative disease in Pediatric Patient. *PET Clin.* 2020;15:309–19. <https://doi.org/10.1016/j.cpet.2020.03.006>
- Nygaard U, Larsen LV, Vissing NH, von Linstow ML, Myrup C, Berthelsen AK, et al. Unexplained fever in children-benefits and challenges of FDG-PET/CT. *Acta Paediatr.* 2022;111:2203–9. <https://doi.org/10.1111/apa.16503>
- Lyra V, Chatziioannou S, Kallergi M. Clinical perspectives for (18)F-FDG PET imaging in Pediatric Oncology: metabolic tumor volume and Radiomics. *Metabolites.* 2022;12. <https://doi.org/10.3390/metabo12030217>
- Masselli G, De Angelis C, Sollaku S, Casciani E, Gualdi G. PET/CT in pediatric oncology. *Am J Nucl Med Mol Imaging.* 2020;10:83–94.
- Mandell GA, Cooper JA, Majd M, Shalaby-Rana EI, Gordon I. Procedure guideline for pediatric sedation in nuclear medicine. Society of Nuclear Medicine. *J Nucl Med.* 1997;38:1640–3.
- Parad RB. Non-sedation of the neonate for radiologic procedures. *Pediatr Radiol.* 2018;48:524–30. <https://doi.org/10.1007/s00247-017-4002-y>
- Lee KH, Ko BH, Paik JY, Jung KH, Choe YS, Choi Y, et al. Effects of anesthetic agents and fasting duration on 18F-FDG biodistribution and insulin levels in tumor-bearing mice. *J Nucl Med.* 2005;46:1531–6.
- Jadvar H, Alavi A, Mavi A, Shulkin BL. PET in pediatric diseases. *Radiol Clin North Am.* 2005;43:135–52. <https://doi.org/10.1016/j.rcl.2004.09.008>
- Juengling FD, Kassubek J, Martens-Le Bouar H, Reinhardt MJ, Krause T, Nitzsche EU, et al. Cerebral regional hypometabolism caused by propofol-induced sedation in children with severe myoclonic epilepsy: a study using fluorodeoxyglucose positron emission tomography and statistical parametric mapping. *Neurosci Lett.* 2002;335:79–82. [https://doi.org/10.1016/s0304-3940\(02\)01060-1](https://doi.org/10.1016/s0304-3940(02)01060-1)
- Saba W, Goutal S, Kuhnast B, Dolle F, Auvity S, Fontyn Y, et al. Differential influence of propofol and isoflurane anesthesia in a non-human primate on the brain kinetics and binding of [(18)F]DPA-714, a positron emission tomography imaging marker of glial activation. *Eur J Neurosci.* 2015;42:1738–45. <https://doi.org/10.1111/ejn.12946>
- Papadopoulos V, Baraldi M, Guilarte TR, Knudsen TB, Lacapere JJ, Lindemann P, et al. Translocator protein (18 kDa): new nomenclature for the peripheral-type benzodiazepine receptor based on its structure and molecular function. *Trends Pharmacol Sci.* 2006;27:402–9. <https://doi.org/10.1016/j.tips.2006.06.005>
- van Rijsewijk ND, van Leer B, Ivashchenko OV, Scholvinck EH, van den Heuvel F, van Snick JH, et al. Ultra-low dose infection imaging of a newborn without sedation using long axial field-of-view PET/CT. *Eur J Nucl Med Mol Imaging.* 2023;50:622–3. <https://doi.org/10.1007/s00259-022-05979-3>
- Reichkender M, Andersen FL, Borgwardt L, Nygaard U, Albrecht-Beste E, Andersen KF, et al. A long Axial Field of View enables PET/CT in Toddler without Sedation. *J Nucl Med.* 2022;63:1962. <https://doi.org/10.2967/jnumed.121.263626>
- Li Y, Wang J, Hu J, Jia J, Sun H, Zhao Y, et al. PET/CT scan without sedation: how to use total-body PET/CT to salvage child's involuntary movement? *Eur J Nucl Med Mol Imaging.* 2023;50:2912–3. <https://doi.org/10.1007/s00259-023-06208-1>
- Olesen OV, Paulsen RR, Hojgaard L, Roed B, Larsen R. Motion tracking for medical imaging: a nonvisible structured light tracking approach. *IEEE Trans Med Imaging.* 2012;31:79–87. <https://doi.org/10.1109/TMI.2011.2165157>
- Kesner AL, Kuntner C. A new fast and fully automated software based algorithm for extracting respiratory signal from raw PET data and its comparison to other methods. *Med Phys.* 2010;37:5550–9. <https://doi.org/10.1118/1.3483784>
- Aide N, Lasnon C, Desmots C, Armstrong IS, Walker MD, McGowan DR. Advances in PET/CT technology: an update. *Semin Nucl Med.* 2022;52:286–301. <https://doi.org/10.1053/j.semnuclmed.2021.10.005>
- Cherry SR, Jones T, Karp JS, Qi J, Moses WW, Badawi RD, Total-Body PET. Maximizing sensitivity to Create New Opportunities for Clinical Research and Patient Care. *J Nucl Med.* 2018;59:3–12. <https://doi.org/10.2967/jnumed.116.184028>
- Zhang Y, Hu P, He Y, Yu H, Tan H, Liu G, et al. Ultrafast 30-s total-body PET/CT scan: a preliminary study. *Eur J Nucl Med Mol Imaging.* 2022;49:2504–13. <https://doi.org/10.1007/s00259-022-05838-1>
- Guo R, Xue S, Hu J, Sari H, Mingels C, Zeimpekis K, et al. Using domain knowledge for robust and generalizable deep learning-based CT-free PET attenuation and scatter correction. *Nat Commun.* 2022;13:5882. <https://doi.org/10.1038/s41467-022-33562-9>
- Nuhn P, De Bono JS, Fizazi K, Freedland SJ, Grilli M, Kantoff PW, et al. Update on systemic prostate cancer therapies: management of metastatic castration-resistant prostate cancer in the era of precision oncology. *Eur Urol.* 2019;75:88–99.
- Lasnon C, Coudrais N, Houdu B, Nganoa C, Salomon T, Eniliorac B, et al. How fast can we scan patients with modern (digital) PET/CT systems? *Eur J Radiol.* 2020;129:109144. <https://doi.org/10.1016/j.ejrad.2020.109144>

24. Zhao YM, Li YH, Chen T, Zhang WG, Wang LH, Feng J, et al. Image quality and lesion detectability in low-dose pediatric (18)F-FDG scans using total-body PET/CT. *Eur J Nucl Med Mol Imaging*. 2021;48:3378–85. <https://doi.org/10.1007/s00259-021-05304-4>
25. Song Xue R, Guo KP, Bohn J, Matzke M, Viscione I, Alberts, et al. A cross-scanner and cross-tracer deep learning method for the recovery of standard-dose imaging quality from low-dose PET. *Eur J Nucl Med Mol Imaging*. 2022;49(6):1843–56. <https://doi.org/10.1007/s00259-021-05644-1>

**Publisher's Note** Springer Nature remains neutral with regard to jurisdictional claims in published maps and institutional affiliations.

Springer Nature or its licensor (e.g. a society or other partner) holds exclusive rights to this article under a publishing agreement with the author(s) or other rightsholder(s); author self-archiving of the accepted manuscript version of this article is solely governed by the terms of such publishing agreement and applicable law.